文章编号：1001-9014(2020)02-0142-07

DOI:10.11972/j.issn.1001-9014.2020.02.002

Optimal theoretical study of the pixel structure and spatio-temporal random noise of uncooled IRFPA

FENG Tao[1], JIN Wei-Qi[1*], SI Jun-Jie[2], ZHANG Hai-Jun[3]

(1. School of Optoelectronics, Beijing Institute of Technology, Key Laboratory of Photoelectronic Imaging Technology and System, Ministry of Education of China, Beijing 100081, China;
2. China Airborne Missile Academy, Henan Luoyang 471009, China;
3. North Guangwei Technology Inc., Beijing 100089, China)

Abstract: The development of uncooled IRFPA pixel structure from a single-layer structure to a double-layer structure reduces noise and improves performance. The pixel structure and its main physical parameters are introduced. It is noted that the main difference between the double-layer structure and the single-layer structure lies in the difference in the effective area of the pixel and thermal conductivity of the bridge leg. The 3-D noise model is an effective method to analyze IRFPA noise, in which spatio-temporal random noise is the main noise part of uncooled IRFPA. The mechanism of spatio-temporal random noise in uncooled IRFPA is analyzed, and a spatio-temporal random noise model is established. The relationship between spatio-temporal random noise, the effective area of the pixel, the thermal conductivity of the leg is obtained. An uncooled IRFPA with a single-layer pixel structure is improved by changing it into a double-layer pixel structure, and the noise is measured. The measured data proved the effectiveness of the uncooled IRFPA spatio-temporal random noise model.

Key words: uncooled IRFPA, spatio-temporal random noise, 3-D noise model, double-layer structure, microbolometer

PACS: 85.60.Gz, 85.85.+j, 07.57.Kp

非制冷 IRFPA 像元结构与时空随机噪声的优化理论

冯 涛[1], 金伟其[1*], 司俊杰[2], 张海军[3]

(1. 北京理工大学 光电学院 光电成像技术与系统教育部重点实验室,北京 100081;
2. 中国空空导弹研究院光电器件研究所,河南 洛阳 471009;
3. 北方广微科技有限公司,北京 100089)

摘要:非制冷红外焦平面探测器(Uncooled IRFPA)像元结构从单层结构向双层结构的发展降低了探测器噪声,提升了性能。介绍了像元的MEMS结构及主要物理参数,指出双层结构与单层结构的主要差异在于像元有效面积和桥臂热导的不同。三维噪声模型是对IRFPA噪声进行分析的有效手段,其中时空随机噪声是非制冷IRFPA最主要的噪声成份。分析了非制冷IRFPA时空随机噪声的产生机理,建立了时空随机噪声模型,得到时空随机噪声与像元有效面积和桥臂热导的关系。将某款单层像元结构探测器改进为双层像元结构并进行噪声测试,实测数据证明了非制冷IRFPA时空随机噪声模型的有效性。

关 键 词:非制冷红外焦平面探测器;时空随机噪声;三维噪声模型;双层结构;微测辐射热计

中图分类号:TN215 **文献标识码**:A

Received date: 2019-06-07, **revised date**: 2019-12-31 **收稿日期**:2019-06-07,**修回日期**:2019-12-31

Foundation items: Supported by Key Projects of the National Natural Science Foundation of China (61231014), Doctoral Fund priority development project of Ministry of Education of China(20131101130002).

Biography: FENG Tao (1977-), male, Ph. D. student. Research area involves uncooled infrared FPA and thermal imaging technology. E-mail: tao.feng@139.com

[*] **Corresponding author**: E-mail: jinwq@bit.edu.cn

Introduction

Infrared thermal imaging technology is used to convert infrared radiation into electronic video images that can be observed by the human eye. The infrared focal plane array (IRFPA) is the core component of an infrared thermal imaging system. Its performance determines the performance of the system. IRFPA can be divided into two types according to the needs of the cooled device: cooled IRFPA and uncooled IRFPA. Cooled IRFPA has high sensitivity and a long detection range, but its structure is complex and expensive. It is usually used in high-end military equipment and space remote sensing. Uncooled IRFPA can work at room temperature without a cooled device, however the sensitivity of uncooled IRFPA is lower than that of cooled IRFPA. Uncooled IRFPA has many advantages, such as fast start-up, low power consumption, small size, light weight, long life, low cost and so on [1]. Therefore, it has been widely used in military and civilian fields.

In recent years, several technologies in uncooled IRFPA, such as the packaging technology, detector materials, microbridge structure, optical resonator, and readout circuit have been improved dramatically [2], which has led to steady improvement in the performance of uncooled IRFPA. It can meet the requirements of most thermal imaging products and has been applied on a large scale by virtue of its cost-performance advantage. The performance improvement in uncooled IRFPA is achieved by improving the signal response ability and reducing the noise level but improving the signal response ability then reduces the signal dynamic range of IRFPA. Therefore, improvements in uncooled IRFPA performance focus on reducing the noise level. In this paper, the pixel structure and the spatio-temporal random noise of uncooled IRFPA are studied. A model for uncooled IRFPA spatio-temporal random noise is established, and a reduction in the spatio-temporal random noise of uncooled IRFPA is realized. This work provides a theoretical basis for further performance optimization of uncooled IRFPA.

1 Pixel structure and noise characteristics of uncooled IRFPA

1.1 Pixel structure of uncooled IRFPA

There are several types of uncooled IRFPA, including thermoelectric stack / thermocouple, pyroelectric, optical mechanical, microbolometer and so on. The microbolometer type has experienced the most rapid development, and it is far superior to other kinds of uncooled IRFPA in its application scope and quantities produced [3]. In this paper, the relationship between pixel structure and the noise characteristics of micrometer uncooled IRFPA is studied.

Figure 1 is the diagram of the single pixel structure of microbolometer IRFPA. The pixel is built on a silicon substrate via MEMS technique. Due to its similarity to a bridge, it is called a microbridge structure, and it is composed of a membrane, leg, pier, and other parts. The

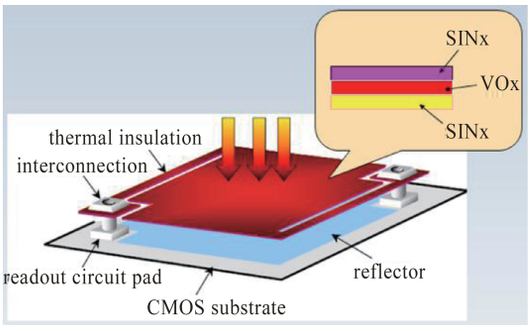

Fig. 1 Structure of the microbolometer [2]
图1 微测辐射热计像元典型结构示意图[2]

membrane is composed of a heat absorption layer and a heat sensitive layer, which acts with a photoelectric signal conversion function, absorbs infrared radiation energy, and converts it to a change in pixel resistance. The leg and pier are composed of supporting material and conductive material. Their functions include supporting the membrane, electrical connection and thermal isolation between the membrane and the substrate.

Optimization of the microbolometer is usually done in two ways: material selection and pixel structure design. The material of the heat absorption layer is required to have a high heat absorption capacity. At present, silicon nitride (SiNx) material is usually used to make the heat absorption layer, which is made in a "sandwich" structure (see Figure 1), and the heat sensitive layer is clamped in the middle of the two heat absorption layers to achieve heat transfer. The heat sensitive layer materials need to have a high temperature coefficient of resistance (TCR), low noise and short thermal time constant. The commonly used materials are vanadium oxide (VO_x) and polycrystalline silicon (a-Si). The MEMS structure of the pixel has an important effect on the performance of the microbolometer. The pixel structure can be divided into single-layer structures and double-layer structures (see Fig. 2). In early uncooled IRFPAs, there was only a one-layer structure over the silicon substrate, and the membrane and leg of the pixel were both located on the same layer. Because of the simple structure and the relative ease of the manufacturing process, the single-layer structure is still widely used. The double-layer structure has two layers above the silicon substrate, the lower layer is the leg layer, and the upper layer is the membrane layer. The design and manufacturing process of the double-layer structure is more complicated than that of the single-layer structure, but uncooled IRFPA products with a double-layer pixel structure have seen rapid development in recent years. Many companies, such as DRS Technologies, Raytheon, NEC Corp., North Guangwei Technology Inc., and Yantai IRay Technology Company, Ltd., have all produced uncooled IRFPA products with a double-layer pixel structure [4-8]. With the increasing scale of uncooled IRFPA resolution and the decrease in the pixel pitch, the performance of the double-layer pixel structure is more apparent than that of a single-layer pixel structure. The dou-

ble-layer pixel structure has become the development trend in uncooled IRFPA pixel structure research.

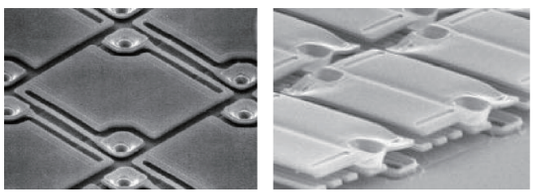

(a) (b)

Fig. 2 Pixel MEMS architecture (a) single layer, (b) double layers
图2 像元MEMS结构(a)单层结构,(b)双层结构

The difference between the double-layer structure and single-layer structure is mainly expressed on the membrane and leg. The effect of the membrane is to absorb infrared radiation and convert heat into the change in value of the pixel resistance. The area of the membrane with infrared absorption ability is called the effective area of the pixel. The larger the effective area, the stronger the absorption ability for infrared radiation. For a single-layer structure, the total area of the pixel is composed of the membrane and leg. Since the leg has almost no infrared absorption ability, the effective area of the pixel is only the membrane part. The leg and membrane of the double-layer structure belong to different layers, and the effective area is almost the same as that of the whole pixel, that is, the double-layer structure usually has a larger effective area than the single-layer structure[9]. The ratio of the effective area to the total area of the pixel is also known as the filling coefficient of IRFPA. For the same pixel pitch, the double-layer structure has a higher filling coefficient than the single-layer structure.

It is in the heat exchange process that the membrane absorbs heat, which results in a change in the resistance of the heat sensitive layer. Therefore, the membrane should have enough thermal capacity to achieve high heat transfer efficiency. The thermal capacity of the membrane is determined by the thermal conductivity between the membrane and the surrounding environment. The thermal conductivity of the membrane mainly includes the contact thermal conductivity between the membrane and the substrate, the convection thermal conductivity between the membrane and the surrounding air, the radiative thermal conductivity of the membrane to the environment, and so on. The pixel of uncooled IRFPA is in a vacuum package and works at room temperature, so the thermal conductivity of the membrane is mainly from the leg, which plays on a mechanical connection between the membrane and the substrate [10]. The lower the thermal conductivity of the leg, the longer the heat holding time of the membrane. However, the lower thermal conductivity of the leg will lead to a larger thermal time constant of the microbolometer, which restricts the frame rate in IRFPA imaging. Therefore, design of the leg thermal conductivity involves a tradeoff. Because the leg in the double-layer structure occupies a single layer, it has more space and flexibility in the leg design than the single-layer structure.

In conclusion, the two-layer structure of uncooled IRFPA pixels is different from the single-layer structure in the effective area of the pixel and thermal conductivity of the leg, which affects the performance of uncooled IRFPA.

1.2 Noise characteristics of uncooled IRFPA

The United States Army's Night Vision and Electronic Sensors Directorate (NVESD) presented a three-dimensional noise model [11] of IRFPA in 1991, which provided a mathematical model for studying the noise characteristics of IRFPA. The core idea of the three-dimensional noise model was to replace the image data of the IRFPA with a combination of one signal component S and seven noise components N_X, which are independent of each other and subject to a Gaussian distribution with a mean value of zero [12]:

$$U(t,v,h) = S + N_T(t) + N_V(v) + N_H(h) + +N_{TV}(t,v) + N_{TH}(t,h) + N_{VH}(v,h) + N_{TVH}(t,v,h) \quad , \quad (1)$$

in the Eq. 1, $U(t,v,h)$ is the function of the three variables in time, vertical direction and horizontal direction[13]. S is the average value of all the data in the three-dimensional image data, corresponding to the response of the signal. The mean value of each noise component, N_T, N_V, N_H, N_{TV}, N_{TH}, N_{VH}, N_{TVH}, is zero, and their root mean squares are represented as σ_T, σ_V, σ_H, σ_{TV}, σ_{TH}, σ_{VH}, σ_{TVH}, respectively. The total noise of the system is expressed as follows:

$$\sigma_{SYS} = \sqrt{\sigma_T^2 + \sigma_V^2 + \sigma_H^2 + \sigma_{TV}^2 + \sigma_{TH}^2 + \sigma_{HV}^2 + \sigma_{TVH}^2} . \quad (2)$$

Among them, T represents the time or frame sequence, and H and V represent spatial dimensions. Seven noise components are described as shown in Table 1 [14]. Each noise component has different sources and forms, and their proportion in the total noise of the detector is different, so the influence on the performance of the detector is not the same.

The more significant noise components of the seven noise components are the spatio-temporal random noise σ_{TVH}, the spatial random noise σ_{VH}, the temporal row noise σ_{TV}, and the spatial column noise σ_H. The spatial random noise σ_{VH} only changes in the direction of row and column, but does not change with time, which affects the output value of different coordinate pixels of IRFPA. It also known as fixed pattern noise, which comes from the difference of signal response between different pixels. The temporal row noise σ_{TV} refers to the fluctuation of the average value of each row with time between frames, also known as time horizontal stripe noise, which mainly comes from the low frequency noise on the bias voltage of detector. The spatial column noise σ_H refers to the fixed non-uniformity between columns, also known as spatial vertical striped noise, which mainly comes from the individual differences between the elements (including blind pixels, integral capacitors, integrators, etc.) shared by each column in FPA.

Because uncooled IRFPA is a staring imaging device, the most important of the seven noise components

Table 1 Description of seven noise components
表1 7种噪声分量说明

Noise Component	Description	Explanation
σ_T	Frame-to-frame noise	Frame average that fluctuates over time.
σ_{TV}	Temporal row noise	The part of the row average that fluctuates over time.
σ_{TH}	Temporal column noise	The part of the column average that fluctuates over time.
σ_{TVH}	Spatial-temporal random noise	The part of each pixel output that fluctuates randomly over time.
σ_V	Spatial row noise	The part of the row average that differs from the spatial distribution.
σ_H	Spatial column noise	The part of the column average that differs from the spatial distribution.
σ_{VH}	Spatial random noise	The part of each pixel output that differs from the spatial distribution.

is the spatio-temporal random noise σ_{TVH} [15], which is the random noise of the output signal in three dimensions: time, horizontal, and vertical [16]. σ_{TVH} represents the fluctuation of pixel output signals between different rows, columns, and frames [17]. σ_{TVH} comes from four kinds of physical noises; thermal noise, flicker noise, temperature fluctuation noise and background fluctuation noise[18].

Uncooled IRFPA, as a microbolometer, converts the thermal radiation signal into an electrical signal by applying a bias voltage pulse on a pixel thermistor, so the thermal noise and flicker noise are the main parts of σ_{TVH} [19]. As shown in Fig. 3 [20], flicker noise is dominant in the low frequency range and thermal noise in the high frequency range. Relatively speaking, the contribution of temperature fluctuation noise and background fluctuation noise to σ_{TVH} is very small, so the two secondary noise sources are not discussed in the following section.

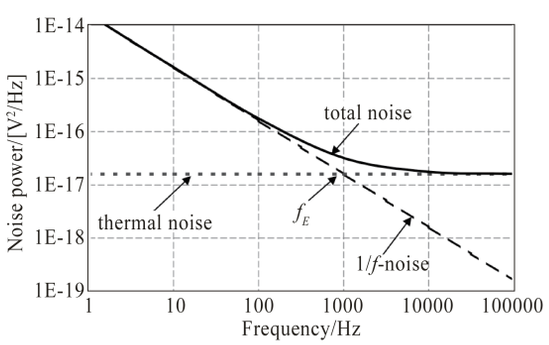

Fig. 3 Noise power density of a semiconductor resistor R=1kΩ
图3 1 kΩ半导体电阻的噪声功率密度

2 Spatio-temporal random noise model of uncooled IRFPA

2.1 NETD of spatio-temporal random noise

The noise of the IRFPA directly affects the performance of the imaging system. The noise equivalent temperature difference (NETD) is a parameter to evaluate the performance of the IRFPA, which combines the noise level and the signal response ability. Because of its clear definition and ease of testing, it has been widely used. The NETD formula for uncooled IRFPA is [20]:

$$\mathrm{NETD}_N = \frac{V_N}{R_V} \quad , \quad (3)$$

where V_N is the noise voltage of IRFPA and R_V is the response rate of the signal voltage.

The NETD model of spatio-temporal random noise can represent the effect of spatio-temporal random noise on the performance of the system.

$$\mathrm{NETD}_{TVH} = \frac{\sigma_{TVH}}{R_V} \quad , \quad (4)$$

where σ_{TVH} is the spatio-temporal random noise voltage of IRFPA.

Since spatio-temporal random noise mainly comes from thermal noise and flicker noise, the following formula is approximate:

$$\sigma_{TVH}^2 = \sigma_J^2 + \sigma_{1/f}^2 \quad , \quad (5)$$

where σ_J is the square root of the IRFPA's thermal noise voltage, and $\sigma_{1/f}$ is the square root of the IRFPA's flicker noise voltage.

The thermal noise equivalent temperature difference of the IRFPA is defined asNETD_J, and the flicker noise equivalent temperature difference of the IRFPA is defined as$\mathrm{NETD}_{1/f}$, which is as follows:

$$\mathrm{NETD}_J = \frac{\sigma_J}{R_V} \quad , \quad (6)$$

$$\mathrm{NETD}_{1/f} = \frac{\sigma_{1/f}}{R_V} \quad . \quad (7)$$

According to Eqs. 4-7, the following formula is obtained:

$$\mathrm{NETD}_{TVH} = \sqrt{\mathrm{NETD}_J^2 + \mathrm{NETD}_{1/f}^2} \quad . \quad (8)$$

2.2 Modeling of the relationship between pixel structure parameters and spatio-temporal random noise NETD

Figure 4 is a schematic diagram of a typical uncooled IRFPA signal conversion circuit. R_s is the sensitive pixel resistor of the uncooled IRFPA for imaging. The external heat radiation energy irradiates up to R_s to change its temperature, which leads to the change in its resistance value. R_d is a blind pixel resistor which is in direct contact with the chip substrate. Its temperature is always equal to the chip substrate temperature and does not change with the external thermal radiation, so its resistance value does not change with the external thermal radiation. In the design of an uncooled IRFPA two-dimensional array, pixels in every column share one R_d.

According to Fig. 4, the expression of the output

signal of IRFPA is:

$$V_o = V_{ref} - \frac{I_{sig}T_{\rm int}}{C_{\rm int}} = V_{ref} - \left(\frac{V_{bd}}{R_d} - \frac{V_{bs}}{R_s}\right)\frac{T_{\rm int}}{C_{\rm int}}. \quad (9)$$

here, V_{ref} is the reference voltage of the integrator; I_{sig} is the integration current; $T_{\rm int}$ is the integration time; $C_{\rm int}$ is the integration capacitance; V_{bd} is the bias voltage applied to R_d; and V_{bs} is the bias voltage applied to R_s.

For the uncooled IRFPA under certain working conditions, V_{ref}, $T_{\rm int}$, $C_{\rm int}$, V_{bd}, V_{bs}, and R_d are independent of the external thermal radiation and can be considered as constants. R_s is a variable that changes with external thermal radiation, and causes the change of output signal V_o, so V_o is a function of R_s.

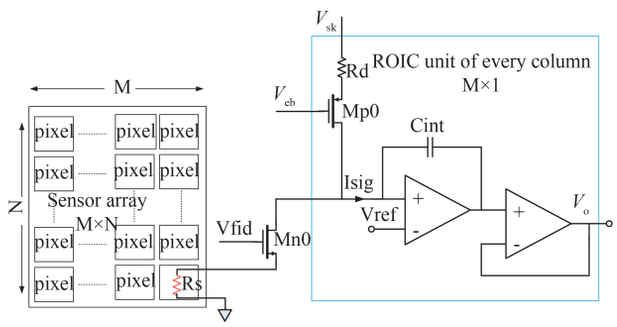

Fig. 4 Signal transfer and readout IC principle diagram of uncooled IRFPA

图4 典型非制冷IRFPA信号转换电路原理图

The voltage response rate of the pixel R_V can be obtained by calculating the derivative of the output signal voltage V_o to the target temperature:

$$R_V = \frac{\delta V_o}{\delta T_t}, \quad (10)$$

where T_t is the target temperature. The target temperature T_t causes the change of pixel temperature T_s through thermal radiation, the change of pixel temperature T_s causes the change of pixel resistance value R_s, and finally the change of pixel resistance value R_s leads to the change in pixel output voltage V_o. Thus, in Eq. 10, the V_o-to-T_t derivation can be converted into a combination of V_o-to-R_s derivation, R_s-to-T_s derivation, and T_s-to-T_t derivation:

$$R_V = \frac{\delta V_o}{\delta T_t} = \frac{\delta V_o}{\delta T_s}\frac{\delta T_s}{\delta T_t} = -\frac{\delta R_s}{\delta T_s}\frac{1}{R_s^2}\frac{V_{bs}T_{\rm int}}{C_{\rm int}}\frac{\delta T_s}{\delta T_t} = -\alpha_s\frac{V_{bs}T_{\rm int}}{R_sC_{\rm int}}\frac{\delta T_s}{\delta T_t}, \quad (11)$$

here, α_s is the TCR of the pixel ($\alpha_s = \frac{1}{R_s}\frac{\delta R_s}{\delta T_s}$).

The thermal noise of an IRFPA pixel is related to the pixel temperature, pixel resistance, bandwidth, and so on. It is expressed as [19]:

$$V_J = \sqrt{4k_B \cdot T_s \cdot R_s \cdot \Delta f}, \quad (12)$$

here, V_J is thermal noise, k_B is the Boltzmann constant; and Δf is the bandwidth of the test system.

By Eqs. 11-12, the thermal noise NETD$_J$ of the IRFPA pixel is:

$$\mathrm{NETD}_J = \frac{V_J}{R_V} = \frac{\sqrt{4k_B \cdot T_s \cdot R_s \cdot \Delta f}}{-\alpha_s \cdot V_{bs}} \cdot \frac{R_sC_{\rm int}}{T_{\rm int}} \cdot \frac{\delta T_t}{\delta T_s}, \quad (13)$$

The flicker noise of the IRFPA pixel is related to the pixel volume, the current flowing through the pixel, the working frequency, and so on. It is expressed as [20]:

$$V_{1/f} = \sqrt{K_{1/f} \cdot I^2 \cdot \ln\frac{f_2}{f_1}} = \sqrt{\frac{K}{v} \cdot \ln\frac{f_2}{f_1}} \cdot \frac{V_{bs}}{R_s}, \quad (14)$$

here, $V_{1/f}$ is flicker noise; I is the current flowing through the pixel; K is the coefficient of flicker noise; v is the pixel volume; and f_1 and f_2 are the lower cut-off frequency and the upper cut-off frequency of the measurement frequency band, respectively.

By Eqs 11-14, the flicker noise $NETD_{1/f}$ of the IRFPA pixel can be obtained:

$$\mathrm{NETD}_{1/f} = \frac{V_{1/f}}{R_V} = -\frac{1}{\alpha_s} \cdot \sqrt{\frac{K}{v} \cdot \ln\frac{f_2}{f_1}} \cdot \frac{C_{\rm int}}{T_{\rm int}} \cdot \frac{\delta T_t}{\delta T_s}. \quad (15)$$

It can be noted that both Eq. 13 and Eq. 15 have the derivation of the pixel temperature T_s of the target temperature T_t, and the relation between it and the pixel parameters is [19]:

$$\frac{\delta T_t}{\delta T_s} = G_{th} \cdot \frac{1 + 4F_n^2}{A\pi\eta} \cdot \frac{\delta T_t}{\delta L_t}, \quad (16)$$

here, $G_{\rm th}$ is the thermal conductance of the pixel; A is the effective area of the pixel; η is the infrared absorption rate of the pixel; F_n is the F number of optics; L_t is the radiance of the target, and the higher the target temperature, the greater the value of L_t.

Equation 16 is substituted into Eq. 13 and Eq. 15. NETD$_J$ and NETD$_{1/f}$ are obtained as follows:

$$\mathrm{NETD}_J = -\frac{1}{\alpha_s}\frac{\sqrt{4k_B \cdot T_s \cdot R_s \cdot \Delta f}}{V_{bs}} \cdot \frac{R_sC_{\rm int}}{T_{\rm int}} \cdot G_{th} \cdot \frac{1 + 4F_n^2}{A\pi\eta} \cdot \frac{\delta T_t}{\delta L_t} = X_J \cdot \frac{G_{th}}{A}. \quad (17)$$

$$\mathrm{NETD}_{1/f} = -\frac{1}{\alpha_s}\sqrt{\frac{K}{v} \cdot \ln\frac{f_2}{f_1}} \cdot \frac{C_{\rm int}}{T_{\rm int}} \cdot G_{th} \cdot \frac{1 + 4F_n^2}{A\pi\eta} \cdot \frac{\delta T_t}{\delta L_t} = X_{1/f} \cdot \frac{G_{th}}{A}. \quad (18)$$

In the formulas, X_J and $X_{1/f}$ are used to replace other parameters independent of A and G_{th}, and the simplified formula can be obtained. Most of the parameters replaced by X_J and $X_{1/f}$ are mainly related to pixel material and working conditions, but have a weak relationship with pixel structure (effective area and thermal conductance of the pixel). Individual parameters, such as pixel volume v, are usually related to pixel effective area A, but in order to simplify the analysis, the pixel volume can be kept unchanged when the pixel effective area is changed, such as reducing the pixel thickness while increasing the pixel effective area, so that the pixel volume

v is also independent of the pixel effective area A.

Equation 19 can be obtained by Eqs. 8, 17-18:

$$\mathrm{NETD}_{TVH} = \frac{G_{th}}{A} \cdot \sqrt{X_J^2 + X_{1/f}^2} \quad . \quad (19)$$

It can be seen that the spatio-temporal random noise of the pixel NETD_{TVH} is inversely proportional to the effective area A of the pixel and is proportional to the thermal conductivity G_{th}. As mentioned earlier, the parameters A and G_{th} are mainly determined by the MEMS structure of the pixel, and the relationship between the pixel structure of uncooled IRFPA and the spatio-temporal random noise can be studied from the two parameters.

3 Experimental verification of the relationship between pixel structure and spatio-temporal random noise

According to the pixel structure and spatio-temporal random noise model of uncooled IRFPA, a typical single-layer uncooled IRFPA is selected to optimize the pixel structure design, and a double-layer pixel structure uncooled IRFPA is developed. The spatio-temporal random noise NETD_{TVH} of the two types of pixel structure are compared to verify the validity of the theoretical model.

3.1 Optimization of uncooled IRFPA pixel structure

GWIR0202X1A is a single-layer uncooled IRFPA product produced by Chinese North Guangwei Technology Inc., as shown in Fig. 5. The thermally sensitive material of the detector is vanadium oxide, the array resolution is 384 × 288, and the pixel pitch is 25 μm.

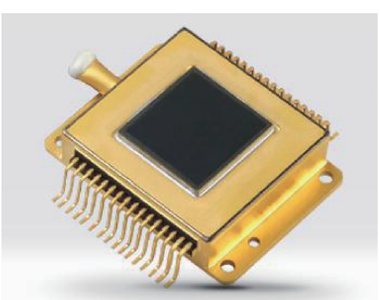

Fig. 5 Uncooled IRFPA GWIR0202X1A
图5 非制冷 IRFPA GWIR0202X1A

Based on GWIR0202X1A, we changed the pixel structure to a double-layer structure, and the other designs such as readout circuit, package and so on, remained the same. The new double-layer structure uncooled IRFPA is called GWIR0202X1A(D). The improvement in performance caused by the change in pixel structure is mainly as follows:

(1)Increase in the effective area of pixel

As mentioned above, the effective area and fill factor of the double-layer structure are larger than that of the single-layer structure. According to the design, the effective area of GWIR0202X1A is about 450 μm^2, and the fill factor is about 72%. The effective area of GWIR0202X1A(D) is about 531 μm^2, and the fill factor is about 85%.

(2)Reduction of the thermal conductivity of the pixel leg

The formula for calculating the thermal conductivity of the pixel leg is as follows:

$$G_{th} = 2 \cdot \frac{\lambda_{th} A_s}{l_s} \quad , \quad (20)$$

here, λ_{th} is the thermal conductivity of the leg, A_s is the cross-sectional area of the leg, l_s is the length of the leg, and the coefficient 2 is because a pixel membrane is supported by two legs.

Without changing the material of the leg, a lower thermal conductivity G_{th} can be obtained by increasing the leg length l_s or decreasing the leg cross-sectional area A_s, but increasing the length or decreasing the cross-sectional area of the leg decreases the mechanical strength of the leg. Compared with GWIR0202X1A, GWIR0202X1A(D) not only increases the leg length l_s but also increases the leg cross-sectional area A_s, while reducing the l_s/A_s value, thus reducing the thermal conductivity G_{th} of the leg, and it maintains sufficient mechanical strength. According to the design, the thermal conductivity of the double-layer structure leg can be reduced to about 80% of that in the single-story structure.

(3)Comprehensive improvement

According to the spatio-temporal random noise model and the relationship between the two pixel structure parameters, the following results can be obtained:

$$\frac{\mathrm{NETD}'_{TVH}}{\mathrm{NETD}_{TVH}} = \frac{A}{A'} \cdot \frac{G'_{th}}{G_{th}} \approx \frac{450}{531} \cdot 80\% = 67.8\%. \quad (21)$$

That is, the double-layer pixel structure NETD'_{TVH} can be reduced to about 67.8% of the single-layer pixel structure NETD_{TVH}. This amplitude of the noise reduction will significantly improve the performance of the IRFPA.

3.2 Experimental verification of the relationship between pixel structure and spatio-temporal random noise

Thirty pieces of single-layer GWIR0202X1A and thirty pieces of double-layer GWIR0202X1A(D) were selected for experimental verification. According to the three-dimensional noise model, the NETD of each noise component and the proportion of the noise components in the total noise energy were obtained, and then calculate the mean value of the samples.

The 3D noise components of single-layer and double-layer IRFPA are shown in Table 2. The NETD_{TVH} of GWIR0202X1A is 30.9 mK, accounting for 52.3% of the total noise energy, so it is the main noise component. After the pixel structure was optimized to a double-layer structure, the NETD'_{TVH} of GWIR0202X1A(D) decreased from 30.9mK to 21.6 mK, which also decreased from 52.3% to 39.2% of the total noise energy. According to the spatio-temporal random noise test result, the ratio of double-layer structure IRFPA to single-layer structure IRFPA is 21.6/30.9=69.9%, which is very close to the theoretical values of Eq. 21 (67.8%). Due to the inherent deviation between process realization and theoretical design, and the inherent difference in the growth of pixel

Table 2 3D Noise test results of single-layer and two-layer uncooled IRFPA
表2 单层结构和双层结构非制冷IRFPA的3D噪声分量测试结果

	3D noise component	σ_T	σ_{TH}	σ_{TV}	σ_{TVH}	σ_H	σ_V	σ_{VH}	σ_{SYS}
Single-layer pixel	The mean of the NETD component/mK	5.0	15.5	4.9	30.9	3.4	7.2	22.8	42.7
	Percentage of noise component to total noise/($\sigma_X^2/\sigma_{sys}^2$)	1.3%	13.2%	1.3%	52.3%	0.6%	2.8%	28.5%	100%
Double-layer pixel	The mean of the NETD component/mK	3.5	14.6	4.3	21.6	3.2	5.8	20.9	34.5
	Percentage of noise component to total noise/($\sigma_X^2/\sigma_{sys}^2$)	1.0%	17.9%	1.5%	39.2%	0.9%	2.8%	36.7%	100%

resistors in different wafer lots, the experimental value (66.9%) is almost consistent with the theoretical calculation value (67.8%). It is proven that the model in this paper is reasonable.

Due to the reduction of the largest noise component σ_{TVH} in uncooled IRFPA noise, the total NETD of IRFPA decreases from 42.7 mK of the single-layer structure to 34.5 mK of the double-layer structure, which effectively improves the performance of the IRFPA. At the same time, it is noted that with the decrease in the spatio-temporal random noise component σ_{TVH}, the proportion of the spatial random noise component σ_{VH} has also increased from 28.5% to 36.7% in the double-layer structure IRFPA. The next step of the study will focus on the spatial random noise component σ_{VH} to explore ways to further improve the uncooled IRFPA performance.

4 Conclusions

Microbolometer uncooled IRFPA is a widely used infrared focal plane detector. The main technical development direction to improve the performance of the uncooled IRFPA is to reduce the noise of the detector. In this paper, a single-layer structure and double-layer structure for uncooled IRFPA pixel are introduced. The effective area of the pixel, the thermal conductivity of the leg and the influence of the largest spatio-temporal random noise component in the three-dimensional noise model are analyzed. The mathematical model of spatio-temporal random noise of uncooled IRFPA is derived. It is pointed out that the effective area of the pixel and the thermal conductivity of the leg are two important parameters in the model. The validity of the model is verified by the experimental testing of single-layer and double-layer uncooled IRFPA.

The uncooled IRFPA of the double-layer structure effectively reduces the spatio-temporal random noise component, which gradually approaches the level of the spatial random noise component. To continue to reduce the noise of uncooled IRFPA, it is necessary to explore the factors of influence given by more noise components, and carry out research on the theory, design and manufacturing process.

Acknowledgment

Hui Fang, Xi He and Guo Tan of North Guangwei Technology Inc. made important contributions to the concept and theoretical analysis of this paper. Qiang Lu and Shuyu Lei provided strong support in the research work. The author would like to express heartfelt gratitude.

References

[1] PU Chao-Guang, HUANG Hui, ZHANG Yu-Long, *et al*. *Uncooled infrared detection material technology* [M]. China: National Defense Industry Press(普朝光, 黄晖,张玉龙,等. **非制冷红外探测材料技术**.国防工业出版社), 2011.
[2] FENG Tao, JIN Wei-Qi, SI Jun-Jie. Uncooled infrared FPA-A review and forecast [J]. *Infrared Technology*(冯涛,金伟其,司俊杰。非制冷红外焦平面探测器及其技术发展动态,**红外技术**), 2015, **37**(3): 177-184.
[3] Rogalski A. Next decade in infrared detectors[J].*Proc. of SPIE*, *Electro-Optical and Infrared Systems: Technology and Applications XIV*, 2017,**10433**: 10433L.
[4] Li C, Han C J, Skidmore G. Overview of DRS uncooled VOx infrared detector development[J]. *Optical Engineering*,2011, **50**(6): 061017.
[5] Murphy D, Ray M, Wyles J, *et al*. 640×512 17 μm microbolometer FPA and sensor development.[J]. *Proc. of SPIE*, *Infrared Technology and Applications XXXIII*, 2007,**65421Z**: 65421Z.
[6] Tohyama S, Sasaki T, Endoh T, *et al*. Uncooled infrared detectors toward smaller pixel pitch with newly proposed pixel structure [J]. *Optical Engineering*, 2013, **52**(12), 123105.
[7] LEI Shu-Yu, FANG Hui, LIU Jun, *et al*. Research on domestic 640×512 uncooled VOx infrared focal plane array [J]. *Infrared Technology*(雷述宇,方辉,刘俊,等. 国产640×512非制冷氧化钒红外焦平面探测器的研制,**红外技术**), 2013, **35**(12): 759-763.
[8] Wang P, Chen S, Gan X, *et al*. High sensitivity 17μm pixel pitch 640 × 512 uncooled infrared focal plane arrays based on amorphous vanadium oxide thin films[J]. *IEEE Electron Device Letters*, 2015, **36**(9): 923-925.
[9] ZHANG Jian-Qi. *Infrared detector* [M]. China: Xidian University Press(张建奇.**红外探测器**,西安电子科技大学出版社), 2016.
[10] Niklaus F, Vieider C, Jakobsen H. MEMS-based uncooled infrared bolometer arrays-review[J]. *Proc. of SPIE*, *MEMS/MOEMS Technologies and Applications III*, 2007, **6836**: 68360D.
[11] D'Agostino J, Webb C. 3-D analysis framework and measurement methodology for imaging system noise[J]. *Proc. of SPIE*, *Infrared Imaging Systems: Design*, *Analysis*, *Modeling*, *and Testing II*, 1991, **1488**:110-121.
[12] CHEN Kai, SUN De-Xin, LIU Yin-Nian. 3D noise model of LWIR system and analysis [J]. *Infrared Technology*(陈凯,孙德新,刘银年. 长波红外系统三维噪声模型及其分析,**红外技术**), 2015, **37**(8): 676-679.
[13] TANG Lin, LIU Lin, SU Jun-Hong. Modeling and simulation research of infrared image noise [J]. *Infrared Technology*(唐麟,刘琳,苏君红. 红外图像噪声建模及仿真研究,**红外技术**), 2014, **36**(7): 542-548.
[14] Sousk S, O'Shea P, Hodgkin V. Measurement of uncooled thermal imager noise[J]. *Proc. of SPIE*, *Infrared Imaging Systems: Design*, *Analysis*, *Modeling*, *and Testing XVI*, 2005, **5784**: 301-308.
[15] Scott L, D'Agostino J. NVEOD FLIR92 thermal imaging systems performance model [J].*SPIE*, *Infrared Imaging Systems*, 1992, **1689**: 194-203.
[16] Yu X N, Nie L G, Hu T L. Model building and measurement of the temporal noise for thermal infrared imager[J]. *Proceedings of SPIE*, *Ninth International Symposium on Laser Metrology*, 2008, **7155**: 71551C.
[17] HU Ming-Peng, MA Dong-Mei, LI Hong-Zhuang, *et al*. The noise model of the staring image system [J]. *Laser & Infrared*(胡明鹏,马冬梅,李宏状,等.凝视型热成像系统噪声模型研究,**激光与红外**), 2007, **37**(9): 863-866.
[18] Rogalski A. *Infraed detectors*[M]. China: China Machine Press (Second Edition), 2014.
[19] Kruse P W, Skatrud D D. *Uncooled infrared imaging arrays and systems* [M].USA: Academic Press, 1997.
[20] Budzier H, Gerlach G. *Thermal infrared sensors: theory, optimisation and practice* [M]. United Kingdom: John Wiley & Sons, Ltd. 2011.